Proceedings of the
Annual Stability Conference
Structural Stability Research Council
San Antonio, Texas, March 19-22, 2024

Influence of end connectivity on the out-of-plane buckling capacity of light-gage steel corrugated panels

Divyansh R. Kapoor[1], Kara D. Peterman[2]

Abstract
Steel deck diaphragms serve as a critical component of a light-gage steel structure's lateral force-resisting system. Design and detailing guidelines for these systems can be found in AISI S310 - 2020 and DDM 04 - 15. The available shear capacity can either be controlled by the limit state of connection failure, or the limit state of panel out-of-plane buckling. While the influence of connection detailing on the connection limit states is well understood, the out-of-plane limit state assumes no change in buckling behavior due to changing end connectivity. This assumption was evaluated through a series of nine full-scale AISI S907 compliant monotonic diaphragm tests. The experimental test matrix included three varying industry-standard support attachment patterns (ex – 36/7, 36/5, 36/4), and all specimens were identical in span length (15 ft), deck type (Type B), and deck gage (22 gage). Results from the experimental study were used to benchmark finite element models capable of capturing buckling behavior and capacity. The developed ABAQUS finite element models utilized idealized non-linear material properties, rigid connection behavior, and contact definitions. The models were used to predict the capacity and buckling behavior of two more commercially available thicknesses (20 gage and 18 gage). Results from the experimental testing and finite element analysis parametric evaluation have been presented in this paper, along with the performance of predictive equations and recommendations on the influence of end connectivity on the out-of-plane buckling limit state.

1. Introduction and motivation

Diaphragms (Figure 1.a) serve as a critical component of a building's lateral force-resisting system (LFRS), transferring lateral loads from the façade of the structure to the designated vertical lateral force-resisting system. Design guidance for profiled steel deck diaphragm panels can be found in AISI S310 – 20 (AISI 2020) and SDI DDM04 (Luttrell 2015) and are controlled by connection limit states or panel buckling limit states. Deck connectivity with the underlying frame can either be fully attached (For example 36/7, Figure 1.b), i.e., connected through the bottom of each flute, or partially attached (for example 36/5 or 36/4, Figure 1.c and Figure 1.d) where not all the flutes are attached to the frame. While adequate design guidance is provided in design codes and manuals such as AISI S310 – 20 (AISI 2020) and SDI DDM04 (Luttrell 2015) to account for the impact of support attachment patterns on the connection limit states, the out-of-plane panel buckling limit state does not consider this impact. Existing research is also limited to the fully attached (36/7)

[1] Ph.D. Candidate, University of Massachusetts, Amherst, dkapoor@umass.edu
[2] Associate Professor, University of Massachusetts, Amherst, kdpeterman@umass.edu

support attachment pattern and no comprehensive dataset exists where tests were specifically designed and performed to study the impact reducing support fasteners (ex. 36/5 and 36/4) can have on buckling capacity and behavior.

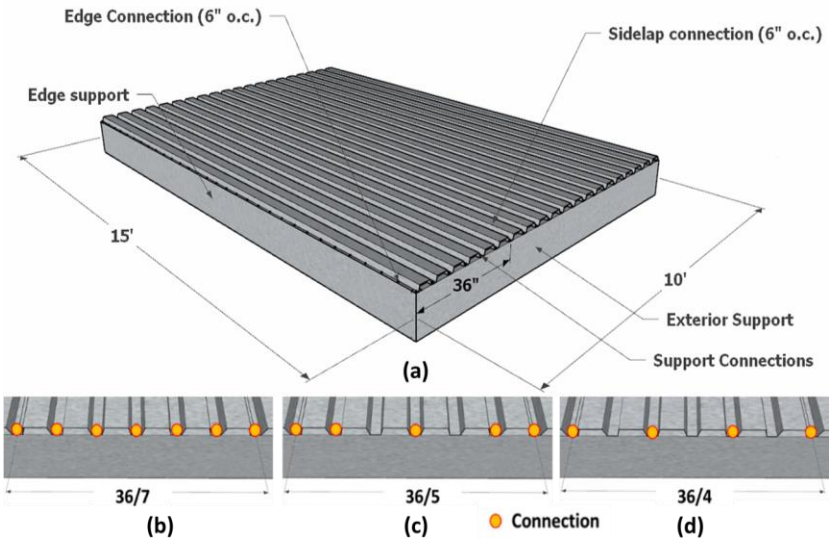

Figure 1: Diaphragm components (a) and typical attachment patterns (b, c, and d)

To further understand the relationship between the support attachment pattern and the out-of-plane buckling limit state, nine monotonic tests were conducted at the University of Massachusetts Amherst Robert B. Brack Structural testing facility. These tests were performed on the cantilever test frame and comprised of three unique configurations with three repetitions each. The specimens were all constructed with 22 gage (0.75 mm) Type B deck (Figure 2) and had identical span lengths (L_v), thickness (t), sidelap connections, edge connections, and only differed in the number of fasteners at the supports to simulate industry standard attachment patterns.

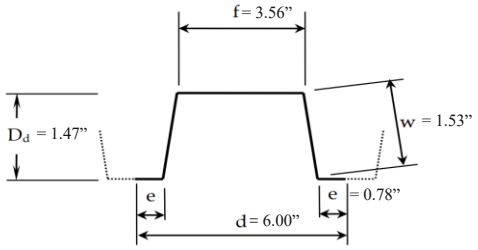

Figure 2: Typical corrugation dimensions for Type B Deck (Luttrell 2015)

2. Review of relevant works

Easley and McFarland (Easley 1975) developed elastic buckling equations to predict critical buckling load of a corrugated metal panel by treating the panels as plates with different flexural rigidities in the two perpendicular directions. The ends were assumed to be simply supported through the mid-plane of every flute, and connections along the panel edges (Sidelap and Edge, Figure 1.a) were assumed to have no impact on capacity. These equations were validated via a suite of eight experimental tests that varied in aspect ratio corrugation pitch, and stiffness in the orthogonal directions. The load was applied via tabs, which were connected to the test specimen on one end and clamped to the test frame on the other. These tab connections were found to have

an end-restraining effect and no longer behaved as purely simply supported connections. The restraining effect of the tabs was accounted for by the end restraint coefficient β which theoretically varied between 1.0 and 1.9 (Easley 1975, Hlavacek 1968). They concluded that the elastic buckling equation was accurate for simply supported panels (β = 1.0), but the true variation of β with end restraint is unknown and depends upon the attachment conditions.

Wright and Hossain (Wright & Hossain 1975) evaluated the impact boundary attachment has on the buckling capacity of profiled sheets while developing analytical models to predict the strength and stiffness of these sheets. Three distinct boundary conditions were analyzed using finite element analysis (FEA) and compared to small-scale tests: welded through both the top flat and bottom flute (Type 1), welded through the bottom flute (Type 2), discretely welded with spot welds in the bottom flute (Type 3). They found that Easley's buckling equations can accurately predict the shear buckling capacity, but needed specific values of β to account for the effect of different boundary conditions i.e., end restraints. The β values back-calculated from FEA and experimental results varied from 1.72, 1.42, and 1.00 for Type 1, Type 2, and Type 3 boundary conditions, respectively. Further, Wright and Hossain also recommended a 50% reduction in buckling capacity if the sheets were only attached in alternate flutes. This 50% reduction also agrees with industry practice and is a significant deviation from recommendations in the code that assumes identical capacity irrespective of end connectivity.

Nunna (Nunna 2011) evaluated the performance of panel buckling equations from TSM (Army, Navy, and Air Force 1982), SDI DDM03 (Luttrell 2004), Easley and McFarland (Easley 1975), and the proposed AISI S310 – 16 (AISI 2016a) equation (Eq. 1). The equations were used to predict the buckling capacities for a historical dataset comprising of twenty-eight full-scale experiments where the failure mode was deck out-of-plane buckling without localized failure of connections. The objective of this work was to evaluate the validity of commonly available panel out-of-plane buckling equations and provide recommendations for resistance factors (LRFD and LSD) and safety factors (ASD). The specimens varied in corrugation depth [1.5 in (38.1 mm) specimen (26 nos.), 2 in (50.8 mm) specimen (1 no.), and 1- 5/8 in (41.3 mm) specimen (1 no.)], corrugation pitch – "d" [6 in (152.4 mm), 9 in (228.6 mm), and 12 in (304.8 mm)], gage – "t" [29 (0.35 mm), 22 (0.75 mm), 20 (0.90 mm), 18 (1.20 mm), and 16 gage (1.52 mm)], number of spans, and span length – "L_v". Twenty-seven of the twenty-eight specimens were fully attached to the test frame with connections through each flute. The strength to predicted ratios for TSM, Easley and McFarland, and current AISI S310 equations can be seen in Figure 3.

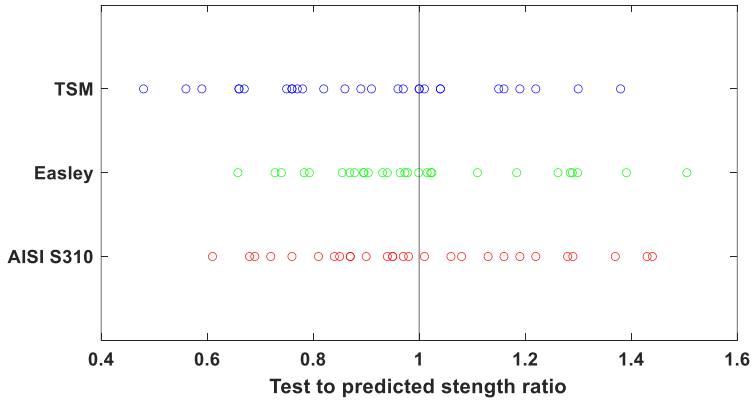

Figure 3: Comparison of existing equations

$$S_{no} = \frac{7890}{\alpha {L_v}^2}\left(\frac{{I_{xg}}^3 t^3 d}{s}\right)^{(0.25)} \quad (1)$$

The equation had an average strength-to-predicted ratio and correlation coefficient of 1.002 and 0.910, respectively, and could be utilized for single and multi-span applications (Nunna 2011). The standard deviation for the strength-to-predicted ratios was 0.213. The calculated LRFD, LSD, and ASD resistance and safety factors were 0.70, 0.55, and 2.27, respectively. Nunna recommended that either the TSM, modified Easley, or proposed AISI S310 equation can be used for estimating the out-of-plane buckling capacity of the deck. However, there was high variability in strength-to-predicted ratios (0.61 – 1.44) for all the out-of-plane buckling equations and majority of specimens were fully attached (27 out of 28).

3. Experimental specimen configuration and test setup

To assess the panel buckling behavior of steel deck with varying end connectivity, an experimental test program (Table 1) was designed which ensured that panel out-of-plane buckling (S_{no}) was the governing failure mode across the attachment patterns. Fully attached (36/7) and partially attached (36/5 and 36/4) support attachment specimens were designed to have significant overstrength in the connection limit states (S_{nf}). The minimum overstrength factor, i.e., the ratio of connection limit state to panel out-of-plane buckling limit state for the configurations, was 1.78. Three repetitions (R1-R3 in Table 1) for each nominally identical configuration were tested. Support and edge fasteners connections were made with #14 (6 mm) screws which had a connection strength (P_{nf}) of 1.24 kips (5.52 kN) each when used with the 22-gage deck (0.75 mm) and 54 mil (1.37 mm) CFS support angles. Sidelap connections were made with the proprietary PunchLok – II® tool which has an individual connection capacity of 2.10 kips (9.34 kN) for the 22-gage (0.76 mm) deck. Sidelaps and edge fasteners were installed 6 inches on center (152.4 mm). Nominal geometric dimensions and material properties [E = 29,500 ksi (203,400 MPa), F_y = 50 ksi (345 MPa), F_u = 65 ksi (448 MPa)] were used for all calculations.

Table 1: Summary of experimental specimen design limit states

Specimen	Attachment Pattern [1,2,3]	L_v (ft)	S_{ni}[4] (klf)	S_{nc}[4] (klf)	S_{ne}[4] (klf)	S_{np}[4] (klf)	S_{nf}[5] (klf)	S_{no} (klf)	S_{nf}/S_{nb} (in)
36/7 - R1									
36/7 - R2	36/7	15.00	2.61	1.82	2.73	2.48	1.82	0.63	2.89
36/7 - R3									
36/5 - R1									
36/5 - R2	36/5	15.00	2.59	1.40	2.68	1.24	1.24	0.63	1.91
36/5 - R3									
36/4 - R1									
36/4 - R2	36/4	15.00	2.54	1.12	2.62	1.24	1.12	0.63	1.78
36/4 - R3									

Notes -

1. Edge and sidelap fastener spacing - 6 in (152.4 mm) on center
2. Exterior edge fastener type - #14 Hex head (P_{nf} = 1.24 kips)
3. Sidelap connections - VSC - II (P_{nf} = 2.10 kips, restricted to 1.24 kips)
4. S_{ni} - Interior connection limit state, S_{nc} – Corner connection limit state, S_{ne} – Edge connection limit state, S_{np} – Perpendicular edge connection limit state
5. S_{nf} – Governing connection limit state [$S_{nf} = \min(S_{ni}, S_{nc}, S_{ne}, S_{np})$]

The fabricated specimens were tested using the UMass Amherst cantilever test frame (Figure 4) which can be used to test specimens in 10 ft X 15 ft (3048 mm X 4572 mm) and 15 ft X 15 ft (4572 mm X 4572mm) configurations. Linear variable differential transducers (LVDTs) were used to measure translations of the test rig and out-of-plane motion of the specimen. Three LVDTs each were located in the north-east and south-west corners of the test frame which measured the X, Y, and Z motion of the rig. Three sensor frames comprising of three LVDTs each were placed along the width of the specimen to measure out-of-plane displacements at various locations during testing. Complete sensor layout and sensor coordinate system can be seen in Figure 4. Specimens were loaded under monotonic loading with a rate of 0.0033 in/sec (0.084 mm/sec) in the negative X direction, until failure.

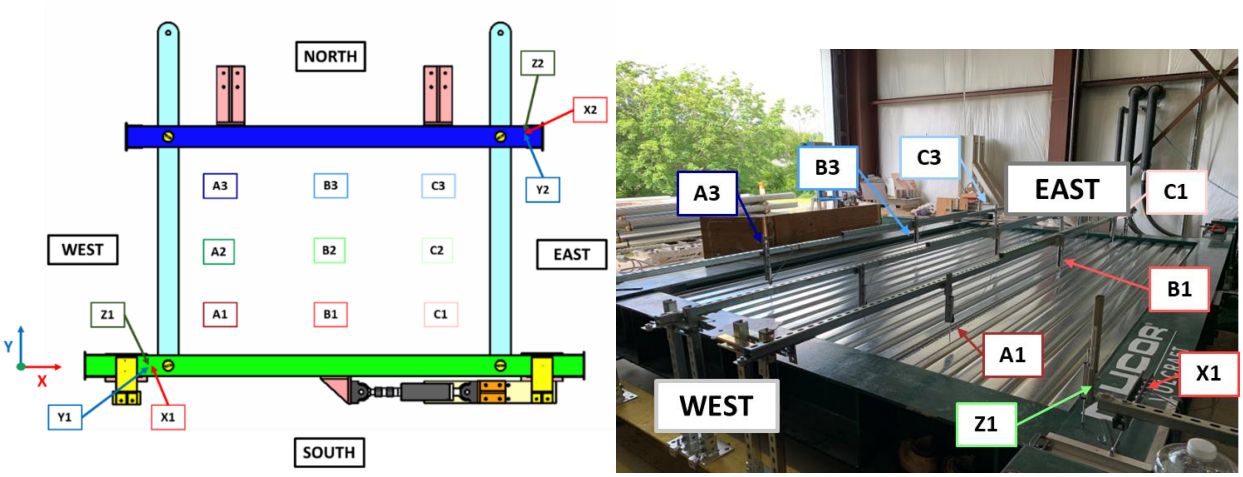

Figure 4: Cantilever test frame and sensor locations

4. Experimental testing results

Experimental testing results of the nine monotonic tests can be seen in Figure 5. Figure 5 shows the force-shear displacement results for all the specimens, accounting for residual test rig movement. The primary failure mode in all repetitions was observed to be deck out-of-plane buckling followed by post-peak connection failures. In general, the test results are repeatable – while specimen 36/5-R2 could not attain the same peak strength as nominally identical specimens, this was attributed to a poor sidelap connection which caused premature failure. The maximum force P_{max}, force at which panel buckling occurred P_{nb}, and force at 40% of P_{max}, P_{40}, are identified in Figure 5. Table 2 summarizes the ultimate capacity, displacement at peak load, and shear stiffness results for each specimen configuration. The displacements recorded by the out-of-plane sensors versus actuator force are shown in Figure 6 for all repetitions. Positive displacements indicate buckling above the deck midplane while negative displacements indicate deck buckling below. The AISI predicted panel buckling capacity ($P_{nb,AISI}$) is indicated by the solid red line. The stiffness (G'_{exp}) of the experimental specimens was calculated using Eq. 2 from AISI S907 (AISI 2017), where a and b are the length and depth of the tested specimen. The comparison between measured stiffness, load at the initiation of buckling, and ultimate load with predictions from AISI S310 – 20 (AISI 2020) can be seen in Table 3.

$$G' = \frac{P_d \times a}{\Delta_d \times b} \tag{2}$$

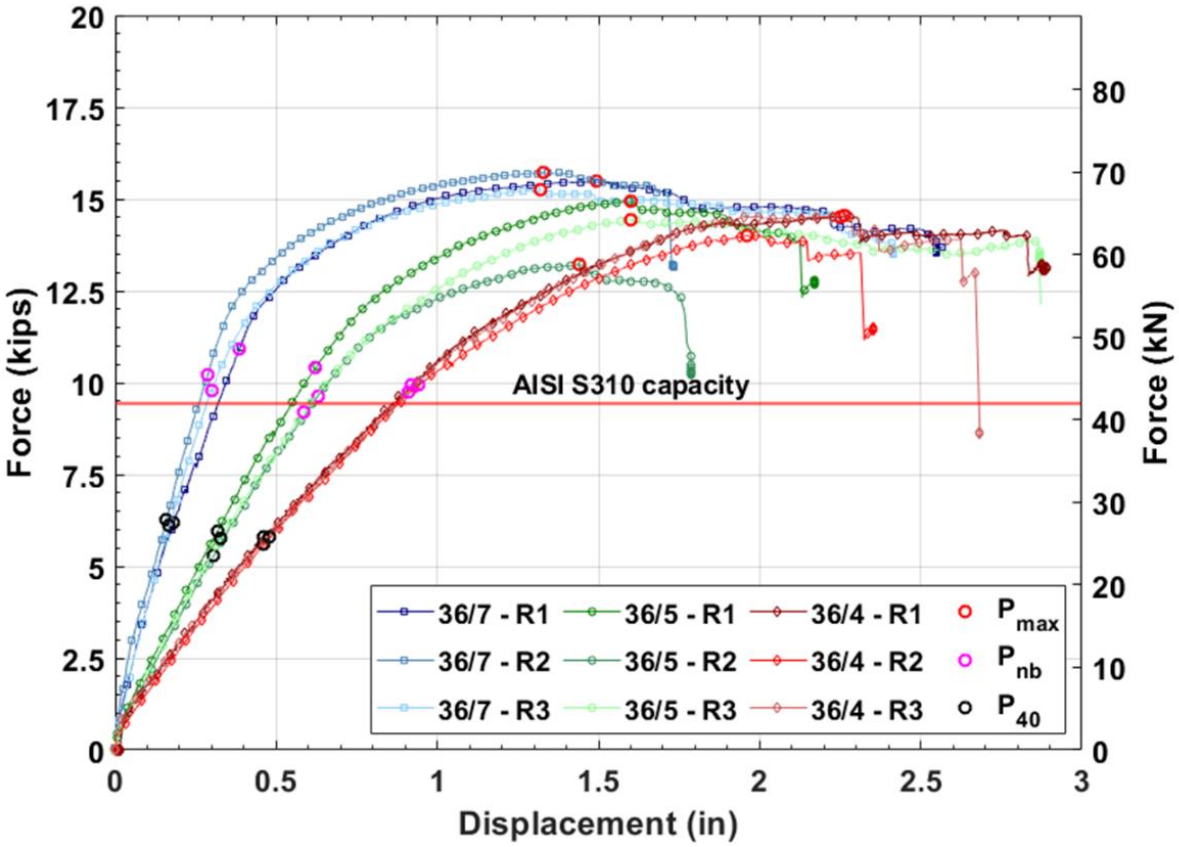

Figure 5: Force-shear displacement behavior across all tested specimens, compared to the AISI S310 predicted capacity (Red solid line)

Table 2: Summary of Results

[Ultimate load and displacement (P_{max} and Δ_{pmax}), initiation of buckling (P_{nb} and Δ_{Pnb}), and stiffness(G')]

Specimen	P_{max} (kips)	Δ_{pmax} (in)	P_{nb} (kips)	Δ_{Pnb} (in)	G' (kips/in)
36/7 - R1	15.5	1.65	10.9	0.38	22.8
36/7 - R2	15.7	1.47	10.2	0.29	26.4
36/7 - R3	15.3	1.38	9.78	0.30	24.2
36/5 - R1	14.9	1.66	10.4	0.62	12.5
36/5 - R2	13.2	1.50	9.62	0.62	11.5
36/5 - R3	14.4	1.69	9.19	0.58	11.7
36/4 - R1	14.5	2.32	9.94	0.92	8.40
36/4 - R2	14.0	2.01	9.93	0.94	8.08
36/4 - R3	14.6	2.31	9.76	0.91	8.12

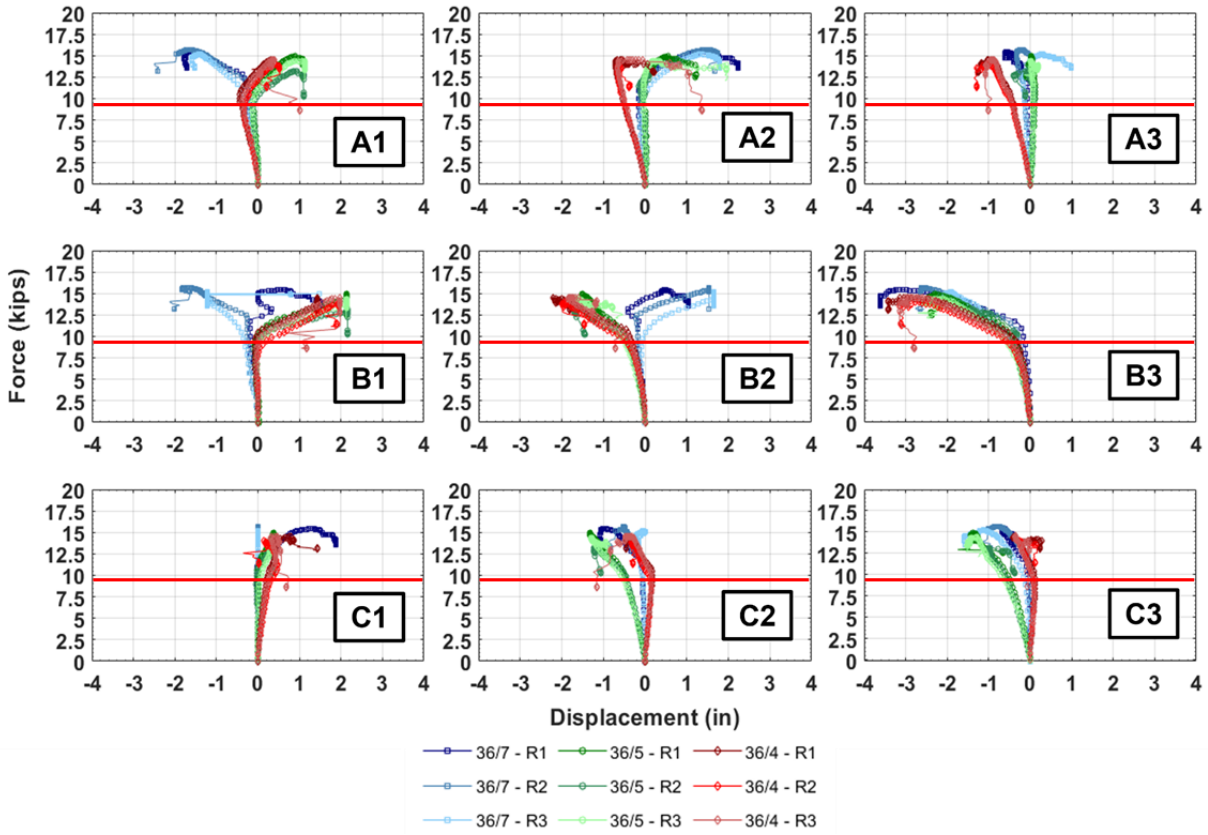

Figure 6: Summary of sensor force-out-of-plane displacement (Δ_z), compared to the AISI S310 predicted capacity (Red solid line)

Table 3: Comparison of P_{max}, P_{nb}, G' with AISI S310 Section D2 and D5 (AISI 2020)]

Attachment pattern	$P_{max,ave}$ (kips)	$P_{nb,ave}$ (kips)	G'_{ave} (kips/in)	$P_{nb,AISI}$ (kips)	G'_{AISI} (kips/in)	$P_{max,ave}/P_{nb,AISI}$	$P_{nb,ave}/P_{nb,AISI}$	G'_{ave}/G'_{AISI}
36/7	15.5	10.3	24.5	9.45	72.9	1.64	1.09	0.34
36/5	14.2	9.74	11.9	9.45	18.7	1.50	1.03	0.64
36/4	14.4	9.88	8.20	9.45	13.6	1.52	1.05	0.60

Changing support attachment pattern had a negligible impact on peak force (P_{max}) observed in the tests, about 7.7% average. When support fasteners were reduced from the 36/7 pattern to the reduced 35/5 and 36/4 patterns, capacity was reduced by 8.3% and 7.3%, respectively. This indicates that the current code assumption that support attachment pattern does not impact peak strength is valid. The average ultimate strength to predicted ratios ($P_{max}/P_{nb,AISI}$) for the 36/7, 36/5, and 36/4 repetitions were 1.64, 1.50, and 1.52 respectively. Changing the support attachment pattern from the 36/7 pattern to the 36/5 and 36/4 pattern reduced the load at which out-of-plane buckling was initiated (P_{nb}) by 5% and 4 %, respectively. The average strength to predicted ratios when comparing initiation of buckling strength with expected capacity ($P_{nb}/P_{nb,AISI}$) for the 36/7, 36/5, and 36/4 repetitions were 1.09, 1.03, and 1.05, respectively. The current code equation was found to be conservative when predicting P_{max}, but accurate for predicting initiation of elastic buckling (P_{nb}).

While the different attachment pattern specimens achieved near identical peak and initiation of buckling capacities, the displacement level at which these capacities were achieved differed vastly (Figure 5 and Table 2). The average displacement at peak force (Δ_{pmax}) increased from 1.50 in (38.1 mm) to 1.62 in (41.1 mm) for the 36/5 specimen, and to 2.21 in (56.1 mm) for the 36/4 pattern tests respectively. This was an increase of 7.8% for the 36/5 and 47.6% for the 36/4 repetitions. This difference was more pronounced when comparing displacement levels at which initiation of buckling was observed. Initiation of buckling was first observed, on average, at a displacement level of 0.32 in (8.22 mm) to 0.61 in (15.41 mm) for the 36/5 specimen, and to 0.92 in (23.5 mm) for the 36/4 pattern tests respectively.

The varying displacement levels had a drastic impact on the specimen's stiffness (Figure 5, Table 2, and Table 3), which indicates the importance of considering attachment patterns for serviceability limit states. This can be observed in the experimental testing results when comparing initial stiffness at the 40% peak load level with the predictive equations from AISI S310 (AISI 2020). As support fasteners were reduced from the fully attached pattern (36/7) to the intermediate (36/5) and skip patterns (36/4), the average stiffness for the set of repetitions (G'_{ave}) reduced from 24.5 kips/in (4.29 kN/mm) to 11.9 kips/in (2.08 kN/mm) and 8.20 kips/in (1.44 kN/mm) respectively. This is a 51% and 67% percent reduction for the 36/5 and 36/4 patterns, respectively, when compared to the fully attached case. The stiffness observed from the experimental tests did not agree well with predictive methods in AISI S310 – 20 Section D5 (AISI 2020) [$mean(G'_{ave}/G'_{AISI}) = 0.52$]. The 36/5 specimens were best predicted [$mean(G'_{ave}/G'_{AISI})_{36/5} = 0.90$] and the fully attached 36/7 specimens had the lowest prediction ratio [$mean(G'_{ave}/G'_{AISI})_{36/7} = 0.34$].

5. Finite element analysis expansion

The experimental results from the full-scale testing were utilized to develop and calibrate finite element analysis (FEA) models capable of capturing experimental strength and buckling behavior observed during testing. The FEA models utilized idealized non-linear material properties, connection behavior, and contact definitions. The calibrated models were used to predict onset of buckling, ultimate capacities, and stiffness for 18-gage and 20-gage Type B deck for comparison with the predictive equation in AISI S310 (AISI 2020) and SDI DDM04 (Luttrell 2015). The numerical modeling matrix for the FEA expansion can be seen in Table 4. To account for the as-modelled geometry of the deck panels in Abaqus (Abaqus 2014), the moment of inertia per unit width (I_{xg}) was estimated by analyzing the deck panels in CUFSM (Schafer & Ádány 2006) for capacity calculations. The 20 gage and 18 gage simulation models are identical to the tested 22 gage specimen in deck profile (Type B), span length (L_v), support member thickness, and attachment patterns (36/7, 36/5, and 36/4) and only differ in the simulated base metal thickness. This ensures that deck thickness is the only variable across the models and the effect of thickness on panel buckling capacity can be isolated.

Table 4: Numerical modeling matrix for FEA Expansion

Specimen	Attachment Pattern	L_v (ft)	Deck Thickness (in)	Support Thickness (in)	$P_{nb,AISI}$ (kips)
36/7 – 22	36/7	15	0.0295	0.054	10.59
36/7 – 20			0.0358		13.84
36/7 – 18			0.0474		21.57
36/5 – 22	36/5	15	0.0295	0.054	10.59
36/5 – 20			0.0358		13.84
36/5 – 18			0.0474		21.57
36/4 – 22	36/4	15	0.0295	0.054	10.59
36/4 – 20			0.0358		13.84
36/4 - 18			0.0474		21.57

5.1 FEA modeling methodology

The FEA model geometry was identical to the tested specimens. Three interconnected full-width [36-inches (914.5 mm)] light gage steel deck panels and one partial panel [12-inches (304.8 mm)] connected to the underlying frame were modeled. The overall size of the FEA model was 10 feet (3048 mm) by 15 feet (4572 mm), as can be seen in Figure 8. The light gage steel deck was modeled with repeating configurations with nominal dimensions provided by the deck manufacturer. The support angles and cold-formed steel (CFS) framing members were modeled based on the nominal dimensions of the framing members used in the experimental testing. An idealized bi-linear material model was utilized to model the nominal stress-strain behavior of steel (Figure 7). The modulus of elasticity, E, and Poisson's ratio were assumed to be 29,500 ksi and 0.3 respectively. Engineering stress and strain were converted to plastic stress and strain to include material plasticity in the models.

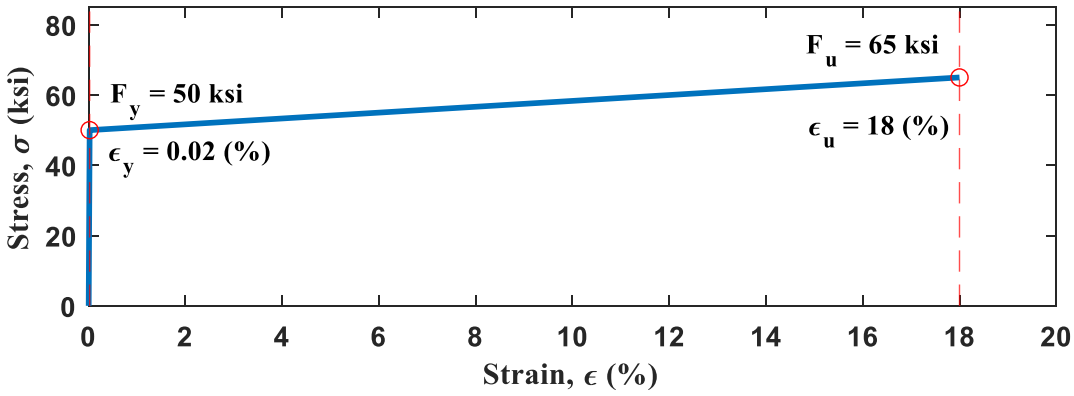

Figure 7: Idealized bi-linear stress-strain curve for FEA simulations

Inbuilt ABAQUS (ABAQUS 2014) multi-point constraints (MPC) and point-based fasteners were utilized in the model to apply boundary conditions and simulate connections respectively. Both the fixed and load joist were constrained to reference nodes located in the middle of the joist webs using MPCs (Figure 8). These reference points were then used to restrict degrees of freedom and apply displacements in the static general load step.

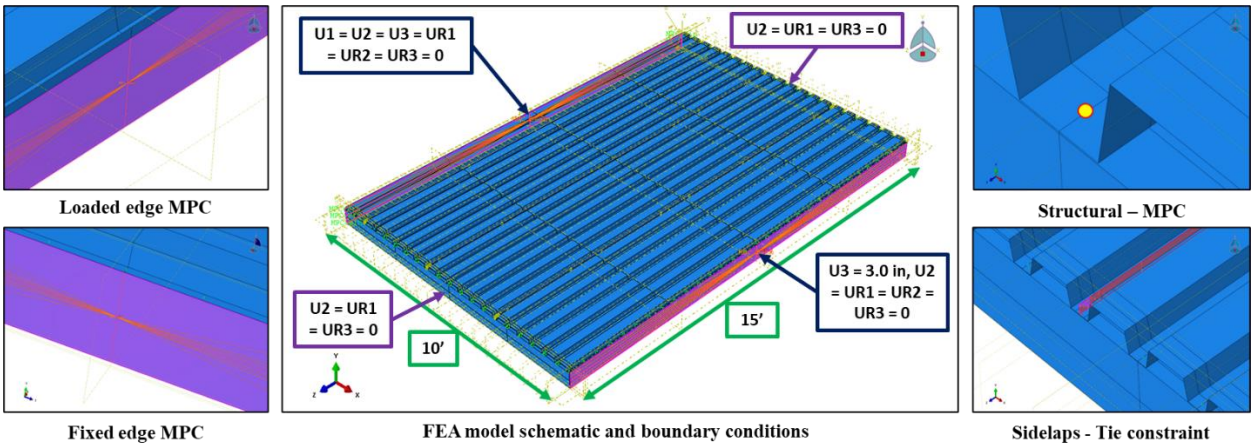

Figure 8: FEA idealization of test specimen, MPC constraints for loaded/ fixed supports and fasteners, and boundary conditions

Connections between the deck and the underlying frame were modelled using the inbuilt Abaqus point-based fasteners (ABAQUS 2014). The fastener behavior in the U1, U2, and U3 directions was defined as a rigid MPC to prevent any slip or deformation at fastener locations. Sidelap connections were not modeled explicitly in the FEA simulations, and a tie constraint was used to join the vertical flats of the panels to simulate the interlocking deck and VSC- II connection (Figure 8). Implications of the structural (frame) fastener and sidelap modelling methodology have been discussed in Section 5.2. Contacts were defined between the ends of the panels and exterior support beams and the bottom flanges of the exterior panels and free and fixed support joist flanges. ABAQUS default "hard" contacts were utilized in the U2 direction and "frictionless" behavior was defined in the U1 and U3 direction (ABAQUS 2014). This was done to prevent the steel panels from penetrating the underlying frame in the FEA models and to simulate realistic warping restraints at the deck ends.

The deck panels were meshed with S4R quadrilateral shell elements with 7 integration points through the thickness. The support angles and CFS members were also modeled with S4R elements. A 0.5 in global mesh size was used to discretize the deck panel and 1.0 in global mesh size was used to discretize the support framing members. The panel mesh size ensured that local buckling was captured by the simulations. A static general load step was defined to incrementally apply the displacement in the FEA simulation. Boundary conditions were imposed on the FEA model by restraining degrees of freedom of the underlying frame to replicate experimental conditions as can be seen in Figure 8. The fixed beam was restricted in all degrees of freedom (U1 = U2 = U3 = UR1 = UR2 = UR3 = 0). The free/load beam was restricted in all degrees of freedom except for U3 and U1 (U2 = UR1 = UR2 = UR3 = 0). Both exterior support beams were restricted by setting U2, UR1, and UR3 = 0 to allow these beams to pivot about their connection to the fixed beam and loaded beam. This also allowed the underlying frame to behave like a pin-jointed frame. A displacement of 3-inches was applied to the free beam in the U3 direction as was done in the experimental tests. The beam was free to move in the U1 direction.

5.2 Comparison with experimental tests

Figure 9 compares the force versus shear displacement response of the FEA models with experimental tests. The FEA models accurately precited peak capacity and mean experimental to

simulated capacity ($P_{max,exp}/P_{max,FEA}$) ratio was 0.95. However, displacement at peak load (Δ_{exp}) was not accurately precited (Table 5) and the mean predicted displacement at ultimate load (Δ_{exp}) versus predicted (Δ_{FEA}) was 1.43. The FEA models were also stiffer (Table 6) than the experimental tests (Mean experimental to FEA precited stiffness ratio, G'_{exp}/G'_{FEA} = 0.78). The error in displacement and stiffness predictions was due to the simplifications made when modeling connection and material behavior.

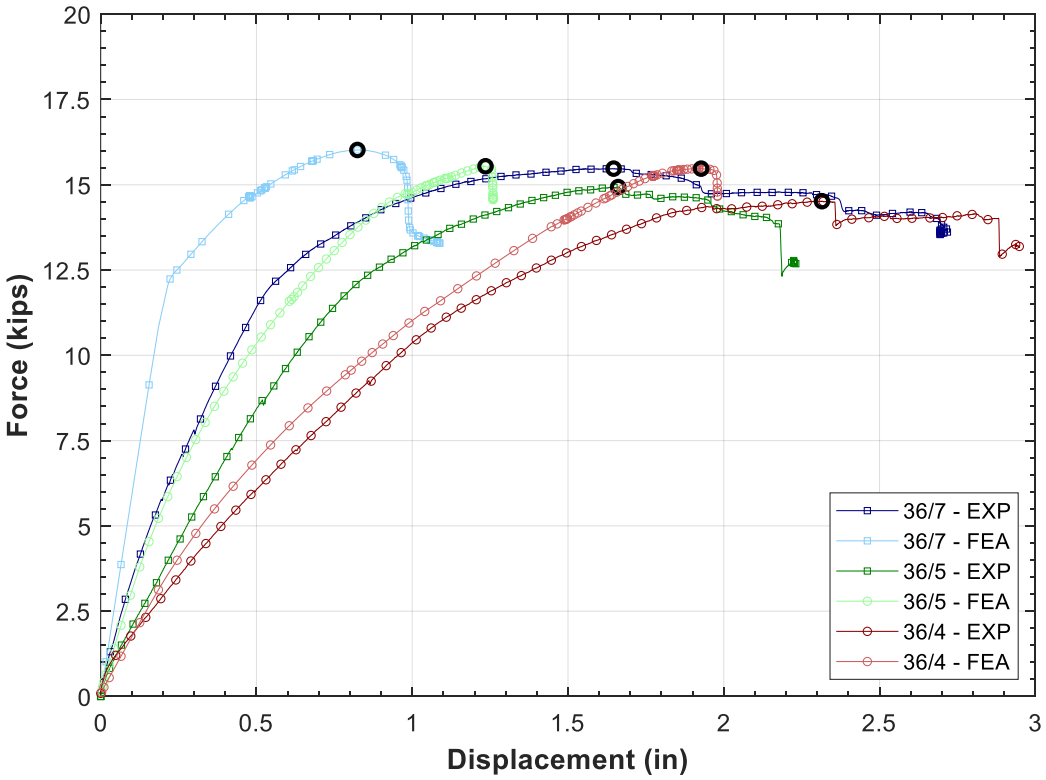

Figure 9:Comparison of experimental and FEA force displacement response

Table 5: Comparison of FEA and experimental peak strength and displacement

Configuration	**$P_{max,exp}$**	**$P_{max,FEA}$**	**$P_{max,exp}/P_{max,FEA}$**	**Δ_{exp}**	**Δ_{FEA}**	**$\Delta_{exp}/\Delta_{FEA}$**
36/7 - 22 gage	15.48	16.02	0.97	1.50	0.82	1.82
36/5 - 22 gage	14.93	15.54	0.96	1.62	1.24	1.31
36/4 - 22 gage	14.36	15.47	0.93	2.21	1.93	1.15
		Mean	0.95			1.43

Table 6: Comparison of FEA and experimental stiffness and reduction in stiffness due to changing fastener pattern

				Reduction in G'			
Configuration	**G'_{exp}**	**G'_{FEA}**	**G'_{exp}/G'_{FEA}**	**Test**	**FEA**	**Description**	**Test/FEA**
36/7 - 22 gage	24.46	34.08	0.72	0.66	0.73	36/7 vs 36/4	0.90
36/5 - 22 gage	11.79	16.89	0.70	0.52	0.50	36/7 vs 36/5	1.03
36/4 - 22 gage	8.24	9.06	0.91	0.30	0.46	36/5 vs 36/4	0.65
						Mean	0.86

Global (out-of-plane) buckling, local buckling, and end-warping behavior observed in the experimental tests were accurately captured by the FEA models and Figure 10 compares the FEA simulations with experimental tests for the 36/4 repetitions. The FEA models accurately predicted overall buckled shapes, local buckling near deck ends, and the end-warping behavior of flutes.

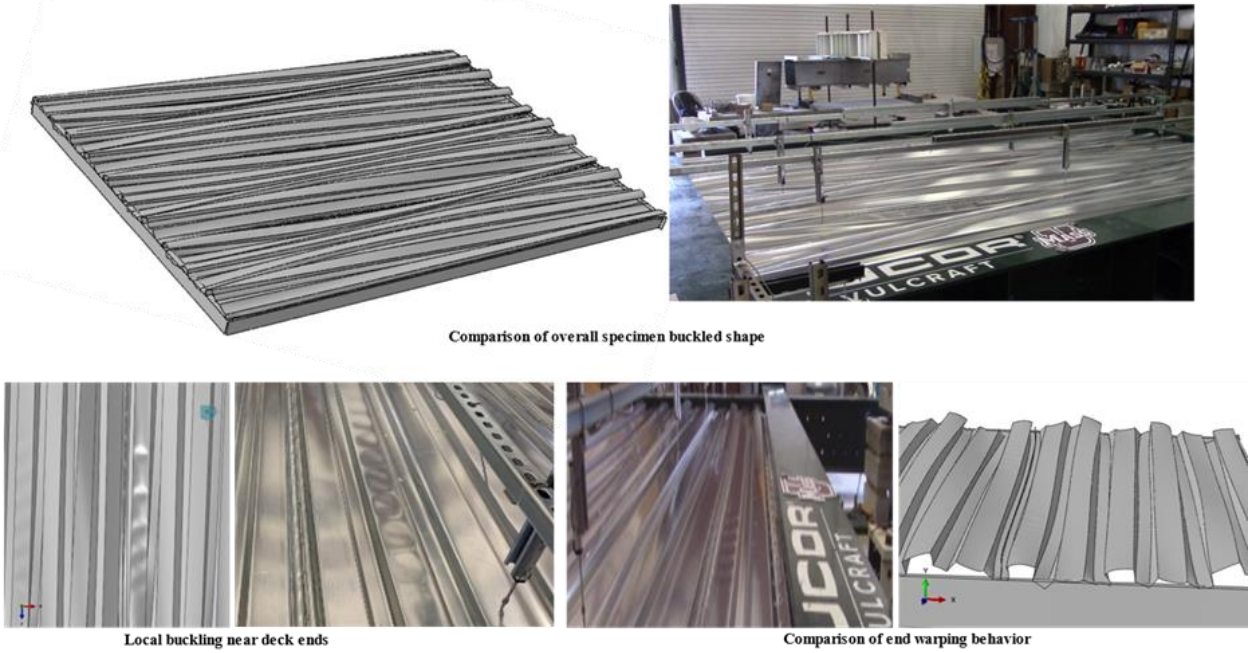

Figure 10: Comparison of FEA and experimental deformed states for the 36/4 skip pattern specimen

Although the FEA models did not accurately capture peak displacement and the stiffness observed during experimental testing, they predicted peak capacities, onset of buckling, and buckling behavior with high accuracy. Further, the models did not require experimentally derived connection or material behavior to make predictions. As the objective of developing these models was to predict capacity of untested configurations, the models were deemed suitable for the FEA expansion.

5.3 Finite element expansion results for the complete modeling matrix

The FEA models developed and presented in Sections 5.1 and 5.2 were utilized to predict capacities for 20-gage and 18-gage Type B decks to evaluate the influence of support attachment patterns across two more commonly used deck thicknesses. The force vs. shear displacement results for the entire parametric evaluation can be seen in Figure 11. Table 7 compares the FEA model predicted ultimate capacities with AISI S310 (AISI 2020) capacity predictions.

For all the configurations, the AISI S310 (AISI 2020) out-plane buckling equation provided conservative estimates for ultimate capacity. The FEA models predicted significant overstrength in the out-of-plane buckling limit state [$mean(P_{max,FEA}/P_{nb,AISI})$ = 1.50], but these capacities were achieved well into the non-linear range of the force-displacement response. Further, there was a drop in capacity in the FEA simulations when comparing the fully attached simulations (36/7) with partial attachments (36/5 and 36/4) for the 18-gage and 20-gage decks. This reduction was about 6% and 17% when comparing the fully attached (36/7) pattern with the intermediate (36/5) and skip (36/4) patterns respectively.

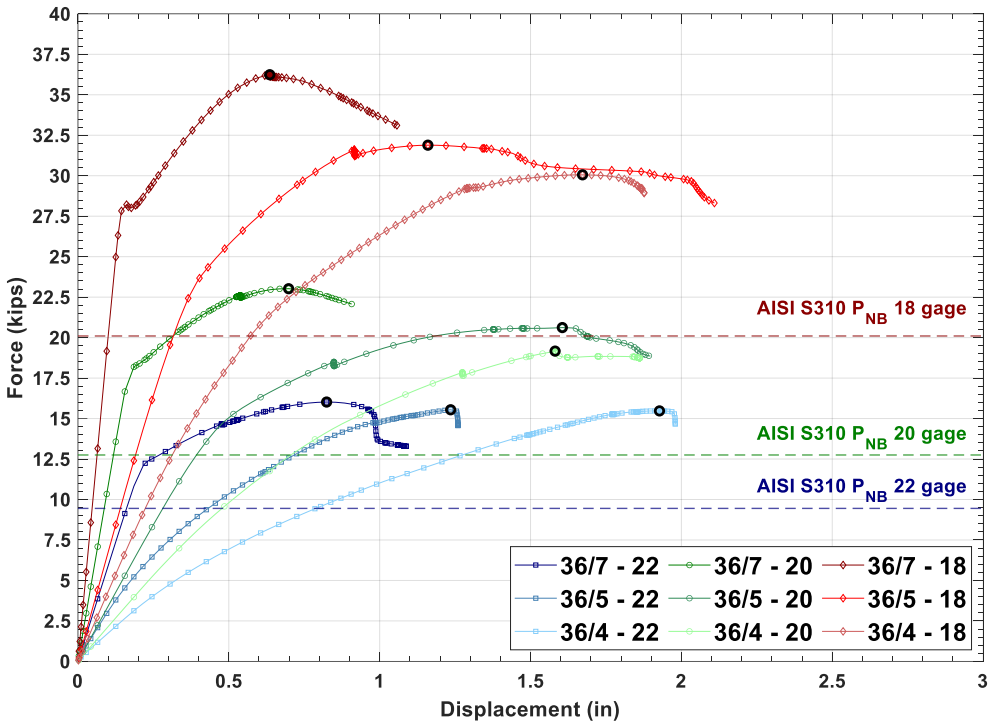

Figure 11: FEA force-shear displacement results summary

Table 7: Comparison of non-linear analysis predicted capacities and AISI S310 -20 Section D2 capacities (AISI 2020)

Configuration	$P_{max,FEA}$ (kips)	$P_{nb,AISI}$ (kips)	$P_{max,FEA}/P_{nb,AISI}$ (--)
36/7 - 22 gage	16.02	10.59	1.51
36/5 - 22 gage	15.54	10.59	1.47
36/4 - 22 gage	15.47	10.59	1.46
36/7 - 20 gage	23.02	13.84	1.66
36/5 - 20 gage	20.62	13.84	1.49
36/4 - 20 gage	19.17	13.84	1.39
36/7 - 18 gage	36.24	21.57	1.68
36/5 - 18 gage	31.89	21.57	1.48
36/4 - 18 gage	30.06	21.57	1.39
		Mean	1.50
		St. Dev	0.10

6. Conclusions

To investigate the influence of end connectivity on the AISI S310 -20 (AISI 2020) and DDM04 panel out-of-plane buckling limit state, nine monotonic tests were conducted. These tests were identical in configuration except for the support attachment pattern. Three unique support attachment patterns were evaluated, and three repetitions were performed for each set. The specimens were instrumented with displacement sensors to capture the onset of buckling. Results from the experimental testing were used to develop an FEA modeling methodology to predict capacity for nine unique configurations. The FEA modeling methodology was validated against

experimental results and utilized non-linear idealized material properties, idealized connection behavior, and contact definitions. The calibrated models were used to predict the ultimate capacities for 18-gage, 20-gage, and 22-gage Type B decks. These simulations were identical in configuration except for the support attachment pattern and base metal thickness. Based on the observations from these experimental tests and numerical simulations, the following key conclusions were drawn:

- Support attachment pattern had negligible impact on the ultimate capacity (7.7%) and load at which buckling initiates (4.5%).
- Reducing support fasteners from the 36/7 pattern to the 36/5 and 36/4 patterns increased displacement at ultimate load level by 7.80% and 47.6% respectively.
- Current design equations provided a conservative estimate for the ultimate capacity of the specimen (Mean test to predicted ratio = 1.55) but provided accurate estimates of the load at which out-of-plane buckling initiated (Mean test to predicted ratio = 1.05).
- Reducing support attachments from the 36/7 pattern to the 36/5 and 36/4 reduced the initial stiffness of the test specimen by 51% and 67% respectively.
- Current design equations provided stiffness estimates that were significantly stiffer than experimental results (Mean test to predicted ratio = 0.52).
- Developed FEA models can capture experimental strength with high accuracy (Experimental/FEA = 95%) and predict buckling (local and global) behavior.
- Stiffness predicted by the FEA models is higher than that observed during experimental testing [mean(Experimental/FEA = 78%)]. This difference is largest for the 36/5 intermediate attached specimen (observed/predicted = 70%).
- Reduction in stiffness when comparing the fully attached specimen with intermediate and skip patterns show good agreement with reductions observed during experimental testing (Experimental/FEA = 90% and 103% for 36/7 versus 36/5 and 36/4 respectively).
- FEA models show similar trends in peak capacity as observed in experimental testing and a significant reserve was observed after initiation of out-of-plane buckling.
- A reduction (6% and 17% average) in peak capacity was observed in the FEA models when comparing the fully attached 36/7 specimens with the 36/5 and 36/4 specimens.

Acknowledgments

The authors gratefully thank the American Iron and Steel Institute (AISI) for their financial support, NUCOR for donation of steel deck and Hilti for donation of fasteners used in the experimental test program. The authors also gratefully acknowledge Brian Bogh, NUCOR, who served as the industry advisor on the project and provided valuable feedback on all phases of the work. Special thanks also go out to Mr. Mark Gauthier, the University of Massachusetts Amherst Structural Engineering and Mechanics lab manager for his help with fabrication and testing.

References

ABAQUS (2014). ABAQUS standard version 6.14-4, Dassault Systems Simulia Corp.

AISI. (2016a). “North American standard for the design of profiled steel diaphragm panels, (AISI S310-16).” American Iron and Steel Institute.

AISI. (2016b). “North American specification for the design of cold-formed steel structural members, (AISI S100-16).” American Iron and Steel Institute.

AISI. (2017). “Test standard for cantilever test method for cold-formed steel diaphragms, (AISI S907).” American Iron and Steel Institute.

AISI. (2020). “North American standard for the design of profiled steel diaphragm panels, (AISI S310-20).” American Iron and Steel Institute.
Army, Navy and Air Force. (1982). “Seismic design for buildings, (Tri-services Manual). Report No. Army TM 5-809-10.” Washington, D.C.: U.S. Government Printing Office.
Easley, J.T. (1975). “Buckling formulas for corrugated metal shear diaphragms.” *Journal of the Structural Division*, 101, 1403-1417.
Hlavacek, V. (1968). “Shear instability of orthotropic panels.” *Acta Technica CSAV*, 1, 134–158.
Luttrell, L.D. (2004). “Diaphragm Design Manual, 3rd Edition (DDM03).” Steel Deck Institute.
Luttrell, L.D. (2015). “Diaphragm Design Manual, 4th Edition (DDM04).” Steel Deck Institute.
Nunna, R, V. (2011). “Buckling of profiled steel diaphragms” Center for Cold-Formed Steel Structures Library. 163
O’Brien et al. (2017). “Characterizing the load-deformation behavior of steel deck diaphragms using past test data.” Cold-formed steel research consortium report series.
Sputo, T. (2017). Steel Deck on Cold-Formed Steel Framing Design Manual (SDCFSFDM), 1st Edition.” Steel Deck Institute
Tao et al (2017). Monotonic and cyclic response of single shear cold-formed steel-to-steel and sheathing-to-steel connections (AISI RP17-2).” American Iron and Steel Institute
Torabian, S., Schafer, B.W. (2021). “Cyclic Experiments on Sidelap and Structural Connectors in Steel Deck Diaphragms.” *Journal of Structural Engineering*, 147, 1403-1417.
Wright, H. D., Hossain, K.M. (1997). “In-plane shear behavior of profiled steel sheeting” *Thin-Walled Structures*, Elsevier, 29 (1-4) 79-100.